ISSN (Print) 1226-1750
ISSN (Online) 2233-6656
Journal of Magnetics 23(2), 229-237 (2018) https://doi.org/10.4283/JMAG.2018.23.2.229

Linear Halbach Structures: The Influence of Different Arrangement and Dimensions on the Resulting Magnetic Field

Václav Žežulka and Pavel Straka*

Institute of Rock Structure and Mechanics, Academy of Sciences of the Czech Republic, v.v.i.
V Holešovičkách 41, 182 09 Prague 8, Czech Republic

(Received 27 November 2017, Received in final form 26 March 2018, Accepted 27 March 2018)

The article presents the results of the experimental implementation of separate and opposing linear structures of different sizes using NdFeB permanent magnets. It focuses on the distribution of the resulting magnetic induction. For both separate and opposing structures, composed of two layers of magnets, the magnetic induction attained was much more affected by changes in the width of the central magnet than by the increasing width of side magnets. When the width of the central magnet in either of the two opposing double-layer Halbach structures was increased approximately three times, the area of the uniform magnetic field attained in the middle of a 20-mm-wide air gap was roughly three times bigger with only ca 7 % lower induction in comparison with opposing Halbach structures of optimized dimensions. These make it possible to generate the maximum magnetic field in the middle of the air gap, but only in a narrow band.

Keywords : magnetic field, permanent magnets, NdFeB magnets, Halbach arrays

1. Introduction

The presented article builds on the previous publication [1], providing the values of magnetic induction obtained for three types of linear opposing arrays from NdFeB permanent magnets. In the publication [1], the opposing structures 1 and 1' (for the separate array 1, see Fig. 1; the separate structure 1' is similar), opposing structures 2 and 1' (a combination of separate Halbach structure 2, see Fig. 2, and the array 1'), and two opposing double-layer Halbach assemblies 2 and 2' (a dimensioned sketch is shown in Fig. 3) were implemented and compared. The dimensions of each of these Halbach structures (including the size of the central block – 15 mm) were selected based on the publication [2], in which Marble has derived the magnetization pattern leading to the strongest stray field at a remote point.

Because of strong interacting magnetic forces, all of these structures were created in a device for the assembly of magnets into two opposing structures (Fig. 4) with a continuously adjustable air gap between them. In this connection, it must also be mentioned that all the separate arrays shown in these as well as other included photographs have been assembled from non-magnetized magnets. After magnetization, these structures can only be assembled using the above-mentioned (or similar) device.

Most studies by other authors have been devoted to cylindrical Halbach structures, but it is indisputable that also linear assemblies have the potential of great practical application, especially thanks to the accessibility of high-quality NdFeB magnets (N45, N50 and N52) [3].

The main reason for further research into the influence of the arrangement and dimensions of the Halbach

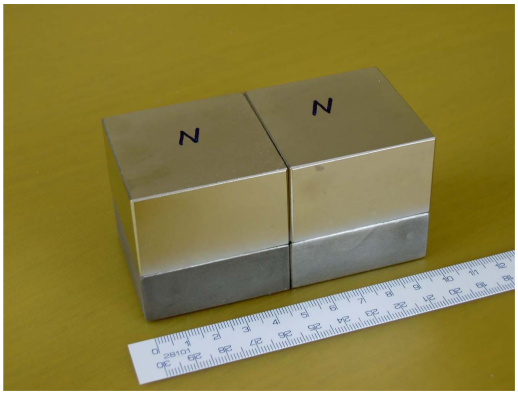

Fig. 1. (Color online) The separate array 1, dimensions: 100 × 50 × 50 mm.

*Corresponding author: Tel: +420-266-009-402
Fax: +420-284-680-105, e-mail: straka@irsm.cas.cz

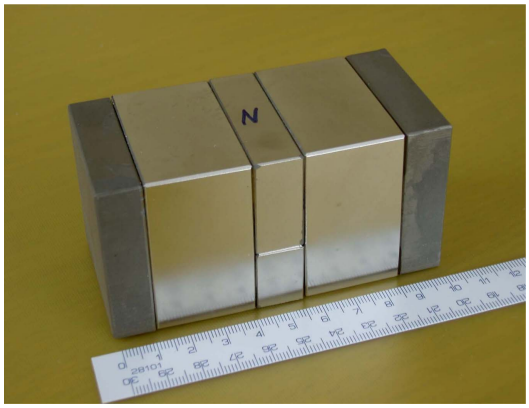

Fig. 2. (Color online) The separate structure 2, dimensions: 100 × 50 × 50 mm.

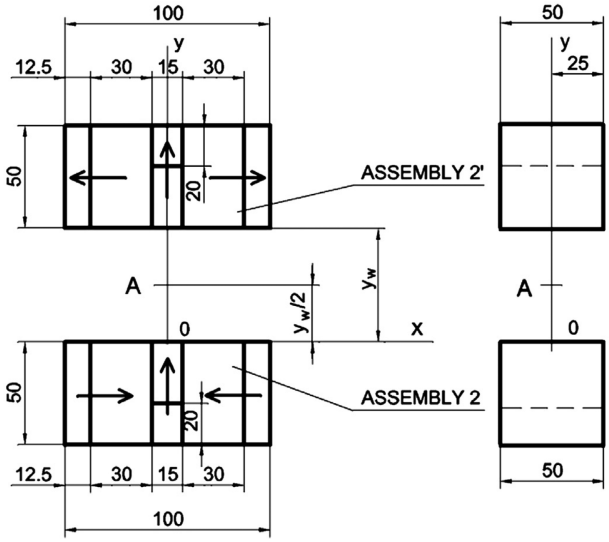

Fig. 3. (Color online) The opposing double-layer assemblies 2 and 2', a dimensioned sketch.

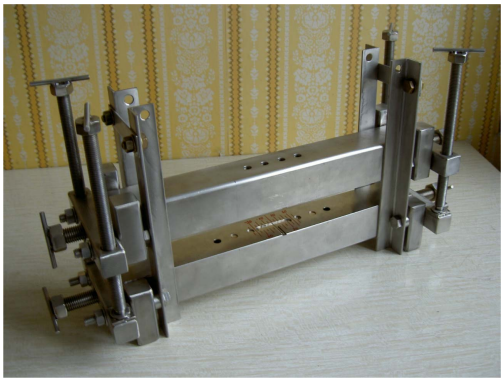

Fig. 4. (Color online) A device for placing NdFeB magnets into two opposing assemblies.

structures assembled from rare-earth magnets on the resulting magnetic field is the significant practical use of these permanent-magnet structures, as arises from the overview below. Attention has been paid to both cylindrical and linear arrangements.

The Halbach structure creates one-sided magnetic flux – on one side of the array, the magnetic field is increased while on the other it is cancelled. Therefore, it has been applied in the magnetic systems of rotating machines, using multipole magnetized rotors [4], and in MRI diagnostic devices. Halbach structures are currently applied mainly in the development of electrodynamic suspensions [5] and DC engines for spacecraft applications [6]. In 2007, however, these structures were first introduced also into HTS Maglev systems for rail transport [7] and subsequently widely accepted, e.g. in Rio de Janeiro for the Maglev-Cobra transportation system [8]. For that reason, the design of structures with one-sided magnetic flux has been devoted great attention.

The designs and optimizations of the structures for the generation of high magnetic fields based on the Halbach cylinder were mainly dealt with by Bloch *et al.* [9], a comparison of the effectiveness of selected types of arrays in the creation of homogeneous fields for MRI-based medical diagnostic devices by Li and Devine [10]. Other studies were focused on the design of Halbach structures by using numerical optimization methods [11], especially on the algorithm for the calculation of the difference between magnetic induction in areas with high and low magnetic fields in an air gap, and on the design of a two-dimensional coaxial Halbach cylinder [12].

Numerous works have been devoted to theoretical designs of permanent-magnet arrays for diverse MRI devices. They were all based on computer simulation. In some cases, also a simple realistic prototype of an array was presented [13, 14]; other works provide mathematical analytical relations for the study of magnetic fields in these devices [15] or describe the properties of various magnetic configurations for MRI [16]. Linear structures find significant use in the purification of raw materials through magnetic separation and filtration as well as in instrumentation [3].

Linear configurations of NdFeB magnets based of Halbach structures for the generation of strong magnetic fields were theoretically modeled [17, 18] and, in some cases, experimentally verified [1]. A comparison of model approaches and results of experiments showed a high correlation between theoretical and experimental results. Both the computer simulation and the implementation confirmed that opposing linear Halbach arrays equipped with NdFeB magnets with a high energy product can provide, in the defined volume, the magnetic induction exceeding the level of the remanent magnetization of the

permanent magnets used. The application of NdFeB magnets of larger sizes or magnetic blocks thus opens a real possibility for the creation of a strong magnetic field in a greater volume for various applications [19].

Considerable attention was paid to simulations of strong magnetic fields. Hilton and McMurry [20] examined a model composed of infinite line dipoles. They carried out computational simulations on a feasible device using the magnetic boundary element method. The resulting arrangement may be used for latching equipment or highly tunable field in the space above the device. Further, optimization methods were used in the design of Halbach arrays to maximize the forces applied to magnetic nanoparticles at deep tissue locations [21]. The methods based on semi-definite quadratic programming yielded optimal Halbach designs in 2D and 3D for the maximum pull or push magnetic forces. Choi and Yoo [11] designed the Halbach magnet array using a numerical optimization method based on finite-element analysis. The optimal magnet arrays composed of two and three linear magnet layers were investigated to increase the attractive, repulsive and tangential magnetic forces between layers. In the work [22], the Halbach permanent magnet designs, in which the magnetic flux density can be altered, were analyzed using numerical simulations and compared with the generated magnetic flux density in a sample volume and the amount of the magnet material used.

The aim of the presented work is to evaluate the influence of the dimensions of the central and side magnets in separate and opposing Halbach structures on the resulting magnetic induction.

2. Computer Simulation

First, the course of magnetic induction in the air gap between the opposing double-layer Halbach structures was simulated. The computational model was formulated based on the definition of the scalar magnetic potential, the zero-divergence condition, the use of a variational approach, and the finite element method application according to [17]. This approach studies two sub-regions: a source-free medium (air) and permanent magnets, while magnetization in the permanent magnets used is homogeneous and air is magnetically isotropic. As starting relations, the definitions of scalar magnetic potential and magnetic induction were considered and the magnetic induction divergence condition respected. A static magnetic field generated by only magnetized bodies is a potential field, and it is possible to introduce a scalar magnetic potential (Φ), defined using magnetic-field intensity $\vec{H}$ as:

$$\vec{H} = -\nabla\Phi \tag{1}$$

Magnetic induction is defined as:

$$\vec{B} = \mu_0\vec{M} + \mu_0\vec{H}, \tag{2}$$

where $\vec{M}$ is magnetization. For the static magnetic field, the magnetic induction must satisfy the zero-divergence condition:

$$\nabla \cdot \vec{B} = 0\,. \tag{3}$$

By inserting the scalar magnetic potential in (2) and combining it with the divergence condition (3), the following equation is obtained:

$$\nabla \cdot \mu_0\vec{M} - \nabla \cdot \mu_0\nabla\Phi = 0\,. \tag{4}$$

Equation (4) constitutes the expression governing a solution of the scalar magnetic potential Φ, while both above-mentioned sub-regions are considered without free currents. Consequently, the tangential components of the magnetic-field intensity along their mutual boundaries are continuous. Nevertheless, the continuity of the normal components $\vec{n}$ of magnetic induction must be claimed. Therefore

$$\vec{n}_1\vec{B}_1 - \vec{n}_2\vec{B}_2 = 0\,, \tag{5}$$

where index 1 refers to the permanent-magnet sub-region and index 2 to the adjacent air sub-region. From (5) and definitions (1) and (2), it follows that

$$\vec{n}\mu_0\vec{M} + \vec{n}\mu_0(-\nabla\Phi_1) - \vec{n}\mu_0(-\nabla\Phi_2) = 0\,, \tag{6}$$

where $\vec{n}$ is the normal unit vector on the interface boundary pointing from sub-region 1 to sub-region 2. Equation (6) represents the boundary state.

Equation (4) can be treated as the governing differential equation on the domain Ω:

$$L\Phi = f. \tag{7}$$

Here, L is the differential operator and f the excitation function. Together with the appropriate boundary condition, it defines a boundary-value problem for the scalar magnetic potential. The solution to this problem can be formulated using the variational approach [17], with no direct solution being used; instead, a functional minimization on the domain Ω is used. Regarding (4), the functional F can be written as:

$$F(\tilde{\Phi}) = \int_\Omega (\nabla \cdot \mu_0\nabla\tilde{\Phi} - \mu_0\nabla \cdot \vec{M})d\Omega = 0\,, \tag{8}$$

where $\tilde{\Phi}$ is an approximate solution to (7). The next step is the use of the Galerkin method to select the weighting

functions for the expansion of an approximate solution [18].

In the *e*-th element in domain Ω, the approximation of an unknown solution is expressed as:

$$\tilde{\Phi}^e = \Sigma_{j=1}^{n} N_j^e \Phi_j^e = \{N_j^e\}^T \{\Phi^e\} = \{\Phi^e\}^T \{N^e\}, \quad (9)$$

where n is the number of nodes in the element, Φ_j^e is the scalar magnetic potential at the j-th node, and N_j^e is the interpolation function for that node. The whole minimization procedure leads to the linear equation system (10):

$$\Sigma_{j=1}^{M} (K^e \{\Phi^e\} - B^e) = 0. \quad (10)$$

Here, K^e and B^e matrices are obtained using (8) for each element; $\{\Phi^e\}$ denotes the column vector of the values of the scalar magnetic potential for the nodes of the *e*-th element. A summation over *e* is needed due to the total number of elements in the domain Ω. Based on (8), (9) and (10), the course of magnetic induction values in the air gap between two opposing linear Halbach structures shown in Fig. 3 was computed.

The numerical modeling of the course of magnetic induction in the air gap for the double-layer Halbach structure considered (Fig. 3) was carried out by the finite element method using the ANSYS software. The model was designed as nonlinear with the input of magnetic properties using *B*-*H* curves. To obtain the magnetic-flux distribution in the air gap, the tested Halbach double-layer structure was represented by an appropriate 3D model. The magnetic assembly was surrounded by a rectangular air region with infinite elements on its outer boundary to simulate the infinite domain. The geometric dimensions of this region were given by the distances from outer model boundaries to the appropriate magnetic assembly surfaces. These distances were selected as the multiples of magnetic assembly dimensions in *x* and *z*-directions on the one hand and the *y*-size plus half-gap thickness in the *y*-direction on the other, while the value of the multiple varied from 5 to 7. These conditions were checked to secure stable results of the computation. For the same reason, the size and the number of the elements in the model were tested as well. It was found that to ensure the stability of the results, the model must contain approximately 2.5×10^6 elements. (A further increase of the element number does not improve the stability of the results much; moreover, it leads to an excessive increase of computational time.)

Based on these simulation results, the double-layered configuration of NdFeB magnets was subsequently implemented. The magnets considered for the simulation and subsequently used for the implementation were NdFeB blocks from the N45 material with remanent magnetization $B_r = 1.354$ T and the maximum energy product $(BH)_{max} = 348$ kJ/m^3. The dimensions of the blocks were $50 \times 50 \times 30$ mm, with the blocks being preferentially oriented in the direction of the height of 30 mm.

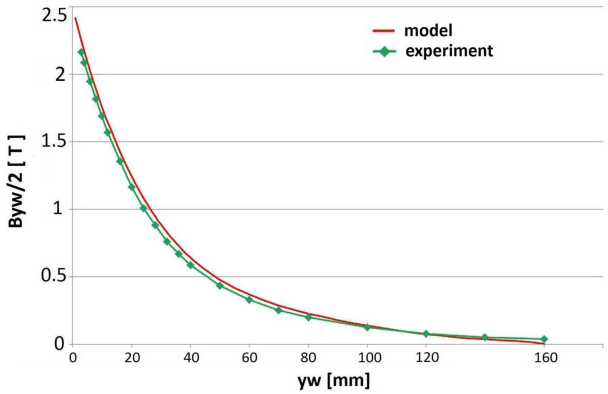

Fig. 5. (Color online) A comparison of the model and experimental course of the magnetic induction in the middle of an air gap along the *y*-axis.

Subsequently, the model courses of magnetic induction were obtained and compared with those achieved experimentally. A comparison of the model and experimental courses of the magnetic induction in the middle of the air gap along the *y*-axis is shown in Fig. 5 [1], whereas a comparison of model and experimental distributions of the magnetic induction in the middle of the air gap along the *x*-axis can be found in Fig. 6. [1] The dependence of magnetic induction on distances from the center of the air gap between two opposing linear Halbach structures (Fig. 3, point A) was modelled by their distancing along the *y*-axis.

It is clear from Figs. 5 and 6 that the model values are in good agreement with the experimental ones. Therefore, based on the mentioned simulation, other similar double-

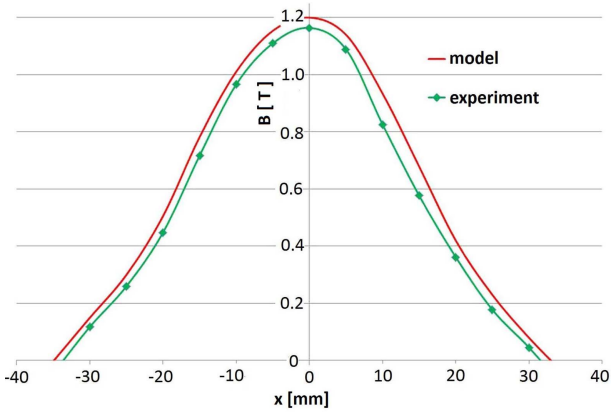

Fig. 6. (Color online) A comparison of the model and experimental distributions of the magnetic induction in the middle of the air gap along the *x*-axis.

layered configurations of NdFeB magnets can be implemented. These configurations are described below.

3. Experimental

During the work, three more opposing Halbach structures of different sizes were gradually created. Each of the opposing arrays was assembled from two separate structures of the same size. Before the separate structures were assembled in the opposing arrangement, the dependences of magnetic induction on the parameters x and y were measured for each of them.

All the arrays were again assembled from NdFeB blocks from the N45 material with remanent magnetization B_r = 1.354 T and the maximum energy product $(BH)_{max}$ = 348 kJ/m^3. Their basis was formed blocks of 0.05 × 0.05 × 0.03 m, preferentially oriented in the direction of the height of 0.03 m. Smaller blocks were created by cutting in such a way that the preferential orientation for the desired magnetization direction would be preserved. In the pictures of all separate structures, some magnetic blocks are Ni coated (light) while others are without this surface layer (dark).

The cross-sections of all the arrays were the same (0.05 × 0.05 m), with only their size along the x-axis changing.

3.1. The Method of Measurement

For the measurements of the dependences in all the arrays, the beginning of the coordinates x and y was always selected in the middle of the surface of the lower structure (point 0 in Fig. 3).

So that the values obtained and the course of magnetic induction would be comparable with earlier results, the measurement methodology used was the same as in the previous work [1]. Magnetic fields in individual configurations were measured with the same teslameter, F. W. Bell, type 5080 with the Hall transverse probe.

For the measurement of the dependence $B_{yw/2} = f(y_w)$, the upper assembly (tube) was moved step by step to the lower one in the bottom tube. With the selected air-gap width y_w, magnetic induction was measured in the middle of the width of this air gap, always using a solid non-magnetic spacer support/pad under the probe. The height of the spacer support/pad was equal to $y_{w/2}$ minus ½ the probe width for its more precise setting.

The dependence $B_{yw10} = f(x)$ was measured with the constant air-gap width w = 20 mm. Magnetic induction was measured in the middle of this air gap at individual points along the x-axis to both the left and right from point 0 according to the scale plotted on the lower as well as upper tubes (see Fig. 4), again while using a solid spacer support/pad under the probe.

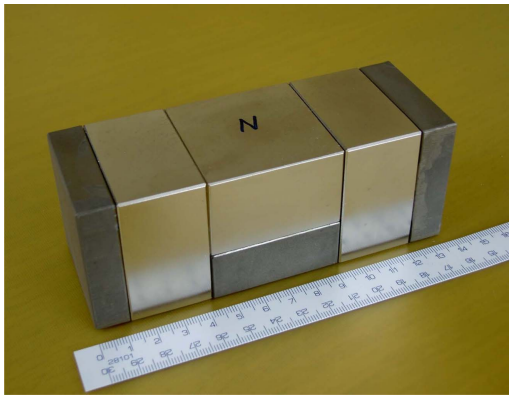

Fig. 7. (Color online) The separate structure 3 of the dimensions 135 × 50 × 50 mm.

3.2. The Opposing Structures 3 and 3'

The separate structure 3 with the dimensions 135 × 50 × 50 mm is shown in Fig. 7. In comparison with the array 2, the central part has been expanded to 50 mm. The structures 3' and 3 are of the same size, magnetized like in Fig. 3.

3.3. The Opposing Structures 4 and 4'

The separate structure 4 of the dimensions 170 × 50 × 50 mm is shown in Fig. 8. The assembly 4' has again the same size as the array 4. Concerning magnetization, the same applies as in the previous case.

3.4. The Opposing Structures 5 and 5'

The separate structure 5 of the dimensions 195 × 50 × 50 mm (Fig. 9) and the assembly 5' also have the same size and have been magnetized in the same way as the structures above.

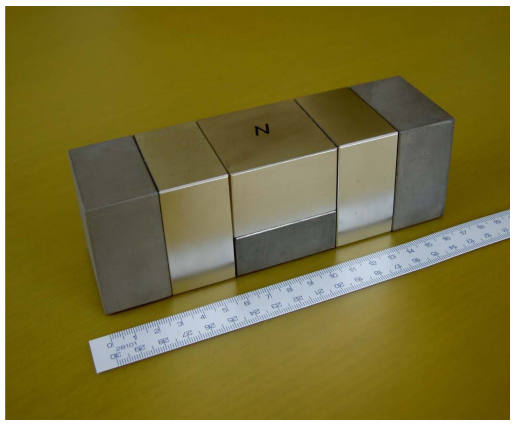

Fig. 8. (Color online) The separate structure 4 of the dimensions 170 × 50 × 50 mm.

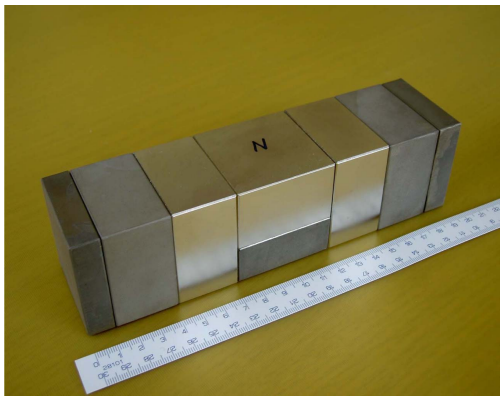

Fig. 9. (Color online) The separate structure 5 of the dimensions 195 × 50 × 50 mm.

3.5. The rules for arrangements of magnets

The arrangement of mentioned assemblies can be briefly summarized in the following points:

– computer simulation,
– selection of magnets,
– cutting some magnets to appropriate dimensions,
– magnetization of individual magnets,
– before the arrays begin to be assembled, the entire device in Fig. 4 is disassembled into individual parts. The two tubes are then moved away from each other to such a distance that prevents the interaction of magnetic forces. Each array is assembled individually and separately.
– assembling of the bottom separate linear Halbach array in the bottom tube of device in Fig. 4 and measurement of the magnetic characteristics of this assembly,
– assembling of the upper separate linear Halbach array in the upper tube of device in Fig. 4 and measurement of the magnetic characteristics of this assembly,
– establishing both tubes with linear Halbach arrays in the device Fig. 4 into the resulting opposite structure and measuring of magnetic characteristics in the air gap.

4. Results

The experimentally determined dependence $B_y = f(y)$ for the separate structure 3 in comparison with the previously published dependence in the case of the assembly 2 is shown in Fig. 10. The dependences $B_{y10} = f(x)$ of the same structures (with B_{y10} measured at the constant distance y = 10 mm from the surface of each array) are shown in Fig. 11.

These dependences were also measured for the separate structures 3' and 2', but the measured values were almost the same as those determined earlier for the structures 3 and 2 (with the deviations being within measurement accuracy). Therefore, they are not listed below.

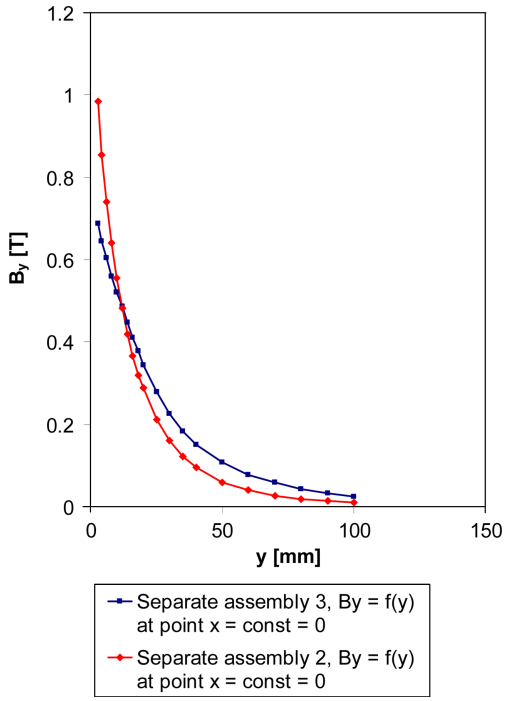

Fig. 10. (Color online) The separate assemblies 2 and 3, the dependences $B_y = f(y)$.

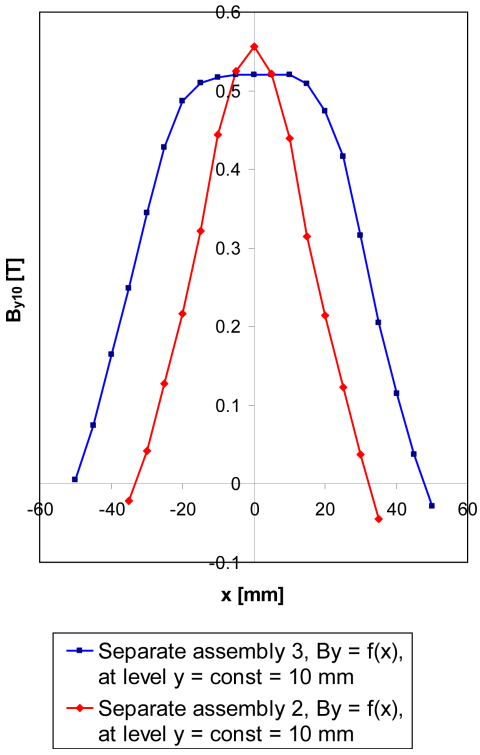

Fig. 11. (Color online) The separate assemblies 2 and 3, dependences $B_{y10} = f(x)$ at level y = const = 10 mm.

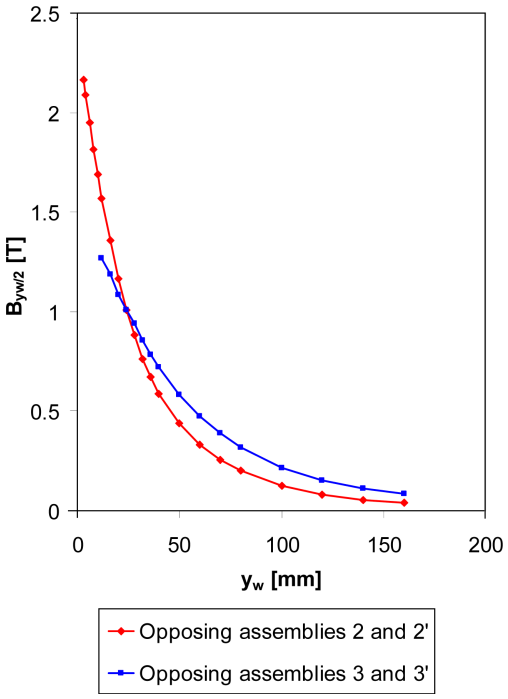

Fig. 12. (Color online) The dependence $B_{yw/2} = f(y_w)$ in the case of the opposing assemblies 2 and 2' and the structures 3 and 3'.

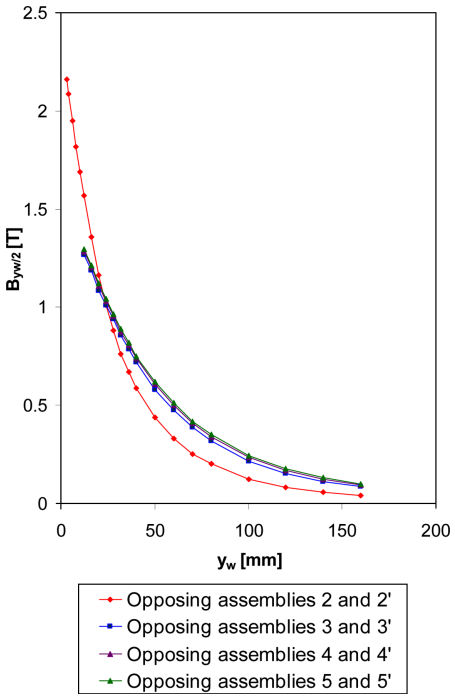

Fig. 14. (Color online) The dependence $B_{yw/2} = f(y_w)$ in the cases of the opposing assemblies 2 and 2', 3 and 3', 4 and 4' and the structures 5 and 5'.

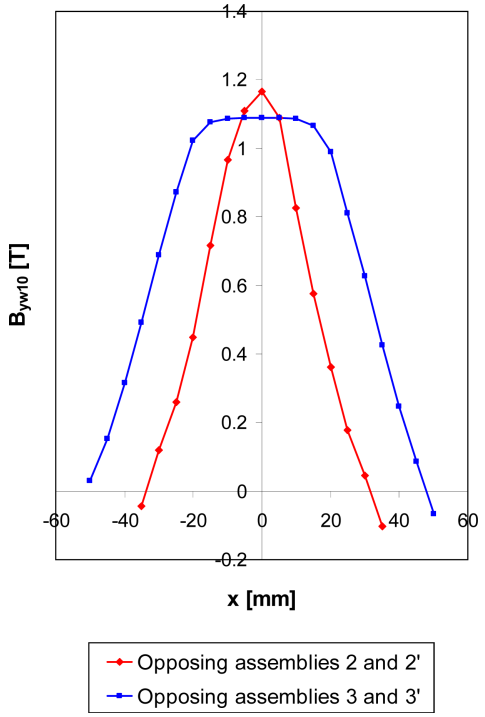

Fig. 13. (Color online) The dependence $B_{yw10} = f(x)$ for y_w = const = 20 mm in the case of the opposing assemblies 2 and 2' and the structures 3 and 3'.

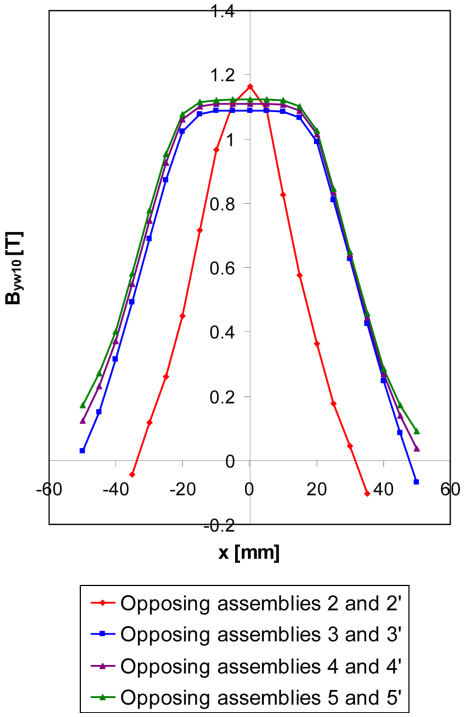

Fig. 15. (Color online) The dependence $B_{yw10} = f(x)$ for y_w = const = 20 mm for the opposing assemblies 2 and 2', 3 and 3', 4 and 4' and the structures 5 and 5'.

So that the above-mentioned dependences could be determined for the separate assemblies 3 and 3'; these structures were placed in the device in Fig. 4 in the opposing position and the dependences $B_{yw/2} = f(y_w)$,

shown in Fig. 12, and the dependence $B_{yw10} = f(x)$, shown in Fig. 13, were measured. For comparison, both figures also depict the relevant dependences of the assemblies 2 and 2'. The same method as in the case of the assemblies 3 and 3' was used to determine the mentioned dependencies also for the opposing structures 4 and 4', 5 and 5'. The dependences $B_{yw/2} = f(y_w)$ of each new assembly (3 and 3', 4 and 4', 5 and 5') including the comparative structure 2 and 2' are shown in Fig. 14. The dependences $B_{yw10} = f(x)$ of all these arrays can be found in Fig. 15.

5. Discussion

A comparison of the magnetic induction B_y attained at the same distance, e.g. 10 mm, from the surface of the magnets for each of the separate assemblies and the same structures in the opposing arrangement (i.e. $B_{yw/2}$ in the middle of the air gap of the width of 20 mm) has confirmed that the magnetic induction attained in the case of the opposing assemblies is more than twice as high. This concerns the comparison of both separate and opposing arrays 2 and 2' and other newly created structures (3 and 3', 4 and 4', 5 and 5'). At smaller widths of the air gap, the magnetic induction obtained, for instance, in the case of the opposing assemblies 2 and 2' can exceed the value of remanent magnetization [1].

It arises from a comparison of the magnetic induction dependences $B_y = f(y)$ for the newly created separate assembly 3 and the comparative separate array 2 (see Fig. 10) that the magnetic induction attained between zero and ca 12 mm from the surface of the magnets is lower than that obtained for the separate assembly 2. At distances greater than 12 mm, on the other hand, it is higher. This is caused by the increased width of the central magnet to 50 mm. The situation is entirely the same for the dependences of the assemblies 3' and 2', which have been measured but are not listed here. When the separate assemblies 4 and 4' (or 5 and 5') are similarly compared with the structures 2 and 2', the intersection point of the two curves is always shifted towards the value of 11 mm.

It is evident from the comparison of the dependences $B_{yw/2} = f(y_w)$ for the opposing assemblies 3 and 3' and the arrays 2 and 2' (see Fig. 12) that the two curves intersect at the air-gap width y_w of approximately 24 mm. When the air-gap width is further increased, the obtained magnetic induction is higher in the case of the opposing assemblies 3 and 3' than in 2 and 2'. The situation is the same in the cases of the arrays 4 and 4' as well as 5 and 5' (see Fig. 14).

The course of the dependences $B_{y10} = f(x)$ with $y = \text{const} = 10$ mm for both the separate assemblies 2 and 3 (see Fig. 11) and the other (not included but measured) separate structures 2', 3', 4, 4', 5 and 5' with a similar course reveals the approximately 7 % higher magnetic induction for the structures 2 and 2' than for newly created assemblies. Nevertheless, this magnetic induction is obtained in a relatively narrow band. On the other hand, the increased width of the central magnet in the newly created separate assemblies makes it possible to expand the area of lower but still very high, relatively uniform magnetic field more than three times.

The previous finding that the area with high and uniform magnetic induction is significantly expanded has been confirmed by the course of the dependence $B_{yw10} = f(x)$ for $y_w = \text{const} = 20$ mm also in the opposing assemblies: 3 and 3' (Fig. 13), 4 and 4', as well as 5 and 5' (Fig. 15).

As already mentioned, when the width of the air gap is larger than 24 mm, the magnetic induction attained in the middle of the air gap is higher in the case of the newly created opposing assemblies than in the comparative opposing structures 2 and 2'. It is evident that also in this case, the area of the uniform magnetic field will be significantly expanded in comparison with these structures 2 and 2'. The requirement to attain the highest possible magnetic field in as large an air-gap volume as possible is thus met even more advantageously in air gaps exceeding 24 mm.

As clear from above, the magnetic induction attained in the newly created Halbach structures is much more affected by the change of the width of the central magnet than by the increasing width of the side magnets. Figures 14 and 15 imply a gradual small increase of magnetic induction in the opposing structures 4 and 4' and 5 and 5' in comparison with the arrays 3 and 3'. Especially in the opposing assembly 5 and 5', however, this increase is so small that it is not important for practical use.

All mentioned findings were obtained using Halbach assemblies of individual magnets $50 \times 50 \times 30$ mm and smaller. It is very likely that the use of larger magnets or blocks would have achieved even greater effects.

6. Conclusions

One of the basic aims of the previous work was to achieve the strongest possible magnetic field in the middle of the air gap between opposing Halbach structures. This work particularly draws attention to the realistically verified finding that when the width of the central magnet in opposing Halbach structures of the same dimensions is increased roughly three times, it is possible to expand the area of the uniform magnetic field in the middle of the

20-mm air gap approximately three times with ca 7 % lower induction than in the opposing Halbach structures. The optimized width of the central magnets in the opposing Halbach structures makes it possible to create a stronger (maximum) magnetic field in the middle of the air gap, but only in a narrow band.

Under the given conditions, the implemented assemblies with small NdFeB magnets can generate relatively high magnetic field with induction exceeding 1.1 T in much larger volume. If this knowledge is applied to analogous opposing Halbach structures with large blocks composed of NdFeB magnets, the effect achieved will undoubtedly be similar. If the previous knowledge were combined with the results obtained when using these large magnetic blocks, the area of the high magnetic field (in this case with the induction of 1.5–1.6 T) would be significantly expanded.

These findings can obviously be applied not only in the treatment and purification of mineral raw materials and various suspensions in the design of magnetic separators and filters, but also wherever a larger volume of high magnetic field is required. It is worth emphasizing again that a magnetic field with these parameters can be created without power consumption, which may become more important in the future as well.

Briefly, the major contributions of the paper are, (a) when the width of the central magnet in opposing Halbach linear structures of the same dimensions increases roughly three times, the area of the uniform magnetic field in the middle of the 20-mm air gap can expand approximately three times (with only slightly lower induction), (b) under the described conditions, the implemented assemblies with small NdFeB magnets can produce a relatively high magnetic field with induction exceeding 1.1 T in a relatively large volume, (c) in the same opposing Halbach assemblies, when increasing the air gap width above 24 mm, the magnetic induction in the air gap is higher than in the comparative separate array.

Acknowledgments

This work was carried out thanks to the support of the Long-Term Project for the Conceptual Development of the Research Organization No. RVO 67985891.

References

[1] V. Žežulka, J. Pištora, M. Lesňák, P. Straka, D. Ciprian, and J. Foukal, J. Magn. Magn. Mater. **345**, 7 (2013).
[2] A. E. Marble, IEEE Trans. Magn. **44**, 576 (2008).
[3] H. Nakamura, Scripta Materialia, in press.
[4] Z.Q. Zhu and D. Howe, IEEE Proc.-Electr. Power Appl. **148**, 299 (2001).
[5] R. Kratz and R. F. Post, IEEE Trans. Appl. Supercond. **12**, 930 (2002).
[6] R. P. Praveen, M. H. Ravichandran, V. T. Sadasivan Achari, V. P. Jagathy Raj, G. Madhu, and G. R. Bindu, IEEE Trans. Ind. Electron. **59**, 3553 (2012).
[7] H. Jing, J. Wang, S. Wang, L. Wang, L. Liu, J. Zheng, Z. Deng, G. Ma, Y. Zhang, and J. Li, Physica C **463-465**, 426 (2007).
[8] G. Sotelo, R. de Andrade, D. H. N. Dias, A. C. Ferreira, F. Costa, O. J. Machado, R. A. H. de Oliveira, M. D. A. Santos, and R. M. Stephan, IEEE Trans. Appl. Supercond. **23**, 3601204 (2013).
[9] F. Bloch, O. Cugat, G. Meunier, and J. C. Toussaint: IEEE Trans. Magn. **34**, 2465 (1998).
[10] Ch. Li and M. Devine, IEEE Trans. Magn. **41**, 3835 (2005).
[11] J. Choi and J. Yoo, IEEE Trans. Magn. **44**, 2361 (2008).
[12] R. Bjørk, C. R. H. Bahl, A. Smith, and N. Pryds, IEEE Trans. Magn. **47**, 1687 (2011).
[13] D. Sakellariou, C. Hugon, A. Guiga, G. Aubert, S. Cazaux, and P. Hardy, Magnetic Resonance in Chemistry **48**, 903 (2010).
[14] Z. Wang, W. H. Yang, X. B. Zhang, L. L. Hu, and H. X. Wang, IEEE Trans. Appl. Supercond. **20**, 777 (2010).
[15] R. Ravaud and G. Lemarquand, Progress in Electromagnetic Research **94**, 327 (2009).
[16] A. Podol´skii, IEEE Trans. Magn. **34**, 248 (1998).
[17] J. Jin, J. Wiley & Sons Inc., New York (2002).
[18] O. C. Zienkiewicz, R. L. Taylor, and J. Z. Zhu, 6th Edition, Butterworth-Heinemann, Oxford (2005).
[19] V. Žežulka and P. Straka, J. Magn. **21**, 364 (2016).
[20] J. E. Hilton and S. M. McMurry, J. Magn. Magn. Mater. **324**, 2051 (2012).
[21] A. Sarwar, A. Nemirovski, and B. Shapiro, J. Magn. Magn. Mater. **324**, 742 (2012).
[22] R. Bjørk, C. R. H. Bahl, A. Smith, and N. Pryds, J. Magn. Magn. Mater. **322**, 3664 (2010).